A Single Intravenous rAAV Injection as Late as P20 Achieves Efficacious and Sustained CNS Gene Therapy in Canavan Mice

Seemin Seher Ahmed[1,2], Huapeng Li[1,2], Chunyan Cao[1,3], Elif M Sikoglu[4,5], Andrew R Denninger[6], Qin Su[1], Samuel Eaton[6], Ana A Liso Navarro[4,5], Jun Xie[1,2], Sylvia Szucs[7], Hongwei Zhang[1,2,10], Constance Moore[4,5], Daniel A Kirschner[6], Thomas N Seyfried[6], Terence R Flotte[1,2,8], Reuben Matalon[7] and Guangping Gao[1,2,9]

[1]Gene Therapy Center, University of Massachusetts Medical School, Worcester, Massachusetts, USA; [2]Department of Microbiology & Physiological Systems, University of Massachusetts Medical School, Worcester, Massachusetts, USA; [3]Department of Physiology, Tongji Medical School, Tongji University, Shanghai, China; [4]The Center for Comparative Neuroimaging, University of Massachusetts Medical School, Worcester, Massachusetts, USA; [5]Department of Psychiatry, University of Massachusetts Medical School, Worcester, Massachusetts, USA; [6]Biology Department, Boston College, Chestnut Hill, Massachusetts, USA; [7]Department of Pediatrics, Biochemical and Molecular Genetics, University of Texas Medical Branch, Galveston, Texas, USA; [8]Department of Pediatrics, University of Massachusetts Medical School, Worcester, Massachusetts, USA; [9]Key Laboratory of Biotherapy, West China Hospital, Sichuan University, Chengdu, Sichuan, China; [10]Current address: South Dakota State University, Brookings, South Dakota, USA

Canavan's disease (CD) is a fatal pediatric leukodystrophy caused by mutations in aspartoacylase (*AspA*) gene. Currently, there is no effective treatment for CD; however, gene therapy is an attractive approach to ameliorate the disease. Here, we studied progressive neuropathology and gene therapy in short-lived (≤1 month) *AspA*^{−/−} mice, a *bona-fide* animal model for the severest form of CD. Single intravenous (IV) injections of several primate-derived recombinant adeno-associated viruses (rAAVs) as late as postnatal day 20 (P20) completely rescued their early lethality and alleviated the major disease symptoms, extending survival in P0-injected rAAV9 and rAAVrh8 groups to as long as 2 years thus far. We successfully used microRNA (miRNA)-mediated post-transcriptional detargeting for the first time to restrict therapeutic rAAV expression in the central nervous system (CNS) and minimize potentially deleterious effects of transgene overexpression in peripheral tissues. rAAV treatment globally improved CNS myelination, although some abnormalities persisted in the content and distribution of myelin-specific and -enriched lipids. We demonstrate that systemically delivered and CNS-restricted rAAVs can serve as efficacious and sustained gene therapeutics in a model of a severe neurodegenerative disorder even when administered as late as P20.

INTRODUCTION

Canavan's disease (CD) is a rare lethal pediatric leukodystrophy characterized by extensive demyelination, edema, and progressive spongy degeneration of the central nervous system (CNS).[1] Currently, there is no effective treatment. Clinical symptoms include blindness, severe psychomotor retardation and early death.[2–4] CD is caused by autosomal recessive mutations in aspartoacylase (AspA) (EC 3.5.1.15);[5,6] an enzyme that deacetylates N-acetyl aspartic acid (NAA) to produce aspartic acid and acetate.[7,8] Since AspA deficiency causes NAA accumulation mainly in the urine,[5] NAA aciduria provides a unique biomarker for CD.[9]
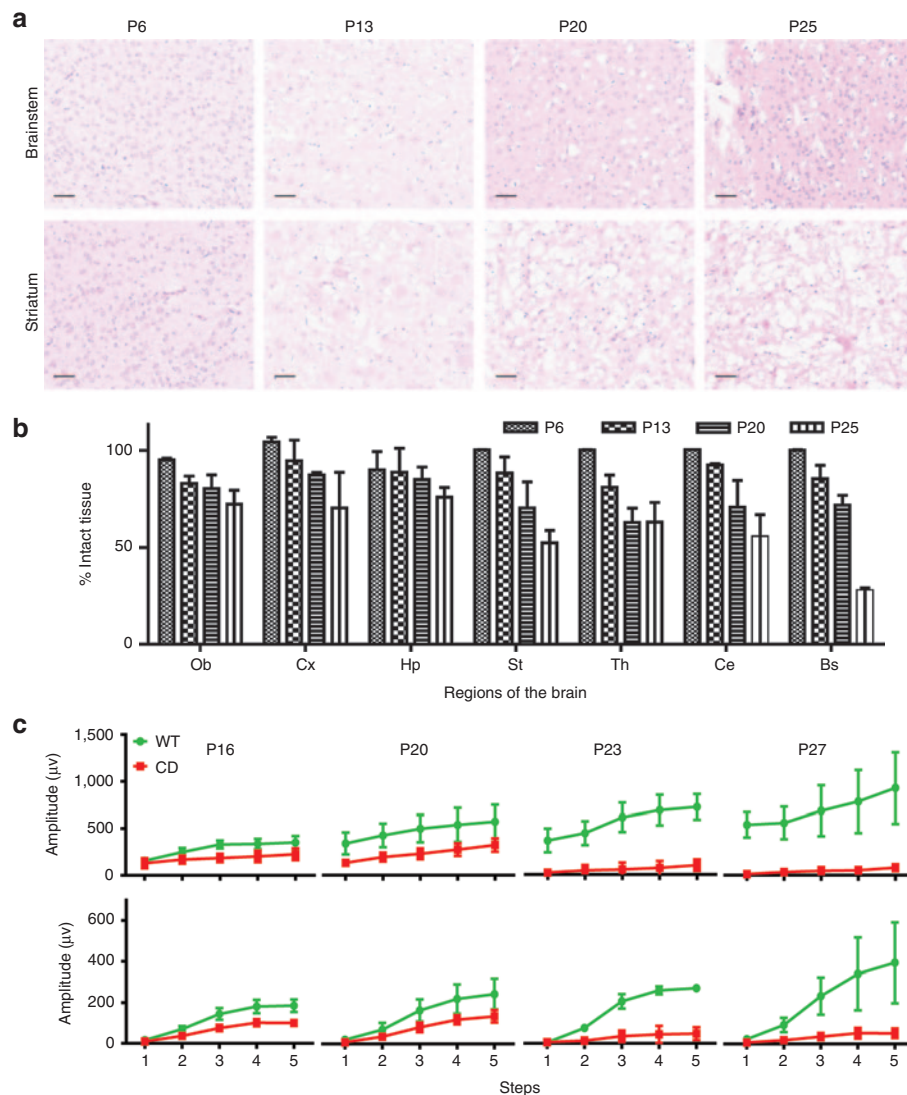
The first *AspA* knockout mouse strain was engineered by an insertional interruption in exon 4 of the *AspA* gene. These mice, also known as CD mice, have a short lifespan (<4 weeks), hydrocephaly, NAA aciduria, extensive white matter vacuolation and motor dysfunction providing a *bona-fide* model to study the severest forms of CD.[10] In addition, there is a naturally occurring CD model, called tremor rat with a large deletion spanning four genes including *AspA* as well as two other more recently created mouse models, all of which have less severe phenotypes and near normal lifespans.[11–13]

Gene replacement therapy is a promising clinical intervention for inborn errors like CD. Novel recombinant adeno-associated viruses (rAAVs) derived from primates represent a promising gene delivery platform because of their wide range of tissue tropism, low immunogenicity, highly efficient and sustained gene transduction, and clinically proven track record in safety.[14–18] In an earlier gene therapy attempt for CD, 23 patients were treated with multiple-site intracranial injections of the first-generation rAAV2.[19] A follow-up study on 13 of these patients revealed the safety of rAAV-mediated therapeutic gene transfer to the CNS over a decade.[20] The treatment resulted in slight reductions of NAA levels in some brain regions; but importantly, it indicated the necessity of early intervention in CD patients.[20] This study also suggests that a global CNS gene transfer is necessary for alleviating widespread neuropathology in CD patients.[19,20]

Correspondence: Guangping Gao, Gene Therapy Center, University of Massachusetts Medical School, 381 Plantation Street, Suite 250, Worcester, Massachusetts 01605, USA. E-mail: Guangping.Gao@umassmed.edu

Thus, one potentially viable strategy for CD gene therapy to target the CNS globally is through intravenous (IV) gene delivery using novel rAAVs that can cross the blood-brain barrier.[21] Based on the initial report on rAAV9,[21] our expanded vector characterization study in neonatal mice[22] as well as preliminary results from a separate comprehensive study to screen rAAVs for IV gene delivery to adult CNS, we selected rAAV9, rAAVrh.8, and rAAVrh.10 for our proof-of-concept gene therapy study. We also designed a therapeutic cassette containing microRNA-binding sites (miRNA-BS) to detarget rAAV expression from peripheral tissues to minimize potentially untoward consequences of IV delivery.

Here, we documented progressive neuropathology and retinopathy in CD mice during early postnatal development. For gene therapy, we tested rAAV9, carrying the human *AspA* gene with and without miRNA regulation in CD mice by IV injections at postnatal day 0 (P0), which restored AspA activity, normalized NAA metabolism, alleviated neuropathy and retinopathy, and improved motor functions. We expanded P0 injection study in CD mice to include rAAVrh.8 and rAAVrh.10, which improved their growth and extended survival up to 2 years (for rAAV9 and rAAVrh.8 groups thus far). Early lethality of CD mice (<4 weeks) was also completely rescued with IV doses of rAAV9 at P6, P13, and even P20, a few days before their death. We also demonstrate that AspA helps to maintain integrity of myelin sheaths and affects the content and distribution of myelin-enriched brain lipids. Most importantly, our study demonstrates, for the first time, an efficacious and sustained IV gene therapeutic for treating terminal stage CD mice as well as successful preclinical *in vivo* application of miRNA-regulated peripheral tissue detargeting in CNS-directed rAAV gene therapy.

Figure 1 Progressive neuropathology and retinopathy in postnatal CD mice. (**a**) Representative images of hematoxyline and eosin (H&E) stained brain sections (*n* = 4). Bars: 4.8 mm. (**b**) Semiquantitative analyses of neuropathology normalized to WT animals using Image J. Ob, olfactory bulb; Cx, cortex; Hp, hippocampus; St, striatum; Th, thalamus; Ce, cerebellum; BS, brain stem. (**c**) Scotopic ERGs of overnight dark-adapted WT and CD mice (*n* = 4 each) to test the response of rods recorded as waveforms (µV) to flickers of light in increasing intensity called steps. CD, Canavan's disease; ERG, electroretinography; WT, wild-type.

RESULTS

AspA deficiency causes progressive neuropathy and retinopathy in early postnatal mice

Histologic examination of the brains from wild-type (WT) and CD mice ($n = 4$ each) at P0, P6, P13, P20, and P25 showed appearance of vacuoles in the CNS of CD but not WT mice at P13, which gradually increased in size and number with age. Neurodegeneration was considered severe by P25 (**Figure 1a**) with afflicted mice dying shortly afterwards. Quantification of intact tissue areas showed progressive pathology in the striatum, thalamus and brainstem (**Figure 1b**), suggesting that AspA helps to maintain CNS integrity.

After full eye opening at P16, WT and CD mice ($n = 4$) were evaluated for retinal response to light flickers by scotopic electroretinography (ERG) at P16, P20, P23, and P27. The ERG trace is produced by the electrophysiological action of the retinal cells and typically consists of a- and b-waves that indicate photoreceptor and glial cell activities respectively. Sequential ERGs revealed progressive reductions in retinal responses of CD mice (**Figure 1c**) indicating the importance of AspA for maintaining visual acuity.

IV injections of rAAV9hAspA and rAAV9hAspA-miRNA-BS reconstitute AspA in the CNS

CD mice injected with rAAV9*hAspA* (CD/rAAV9) at P0 were killed at 3 months to evaluate brain AspA levels by western blot. AspA levels in the gene-corrected (GC) mice were similar to age-matched phenotypically normal heterozygous (Het) mice (**Figure 2a**).

AspA enzyme activity (normalized to WT mice) in brain homogenates of GC mice were similar to Het mice ($P > 0.05$)[23] (**Figure 2b**). To reduce transduction in peripheral tissues such as liver, heart, and skeletal muscle by systemically delivered rAAV9 hAspA, a miRNA-regulated vector genome was designed for CNS-restricted gene transfer.[23] Equal doses of rAAV9*hAspA* and rAAV9*hAspA-(miR-1BS)_3-(miR-122BS)_3* (*i.e.,* rAAV9*hAspA-miRBS*) with three copies each of the miRNA-BS specific to miR-1 and miR-122 (enriched in heart, skeletal muscle, and liver, respectively) were infused into CD mice at P0. Both vectors targeted brain, liver, heart, and muscle tissues equally; but the miRNA-regulated vector abolished AspA expression only in peripheral tissues not the brain (**Figure 2c**), establishing specificity of miRNA-regulated therapeutic expression from rAAV.

Immunohistochemistry illustrated similar numbers and distribution patterns but different staining intensities of AspA-positive cells in the brains of WT and GC mice (**Figure 2d**). Large vacuoles in CD mouse brain sections made detection of residual AspA difficult. Double immunofluorescent staining showed efficient neuronal *AspA* gene transfer by rAAV9 in the cortex, hippocampus, and thalamus in GC mice (**Figure 2e**).

Spectral peak integrals for total NAA (2.02 ppm) and total creatine (tCr, 3.05 ppm)[3,20,24] were determined by acquiring ^{1}H proton magnetic resonance spectroscopy data from live experimental animals ($n = 3$). Abnormally high endogenous NAA levels were detected in CD mice relative to WT mice as expected[10,25] (**Figure 2f**). Integrated values of NAA/creatine ratios were significantly different between WT (0.886 ± 0.03), and CD (2.63 ± 0.16) ($P > 0.001$); such values were reduced in GC mice (2.18 ± 0.64)

(**Figure 2g**). NAA aciduria, a biomarker of CD,[5,10] was significantly reduced in GC mice ($P < 0.001$) compared with CD mice (**Figure 2h**).

AspA gene therapy in CD mice alleviates neuropathology, cerebral edema, and retinopathy

Hematoxylin and eosin stained coronal sections of brain and spinal cord from terminal stage (P27) CD and P90 GC mice were examined (**Figure 3a**) and quantified (**Figure 3b**) for neuropathology. Our data suggest significant improvements in all regions of spinal cord and most regions of the brain. Quantification for total neuronal populations showed no significant impact of white matter degeneration on neuronal survival (data not shown).

T2-weighted magnetic resonance imaging was used to detect cerebral edema[26] in WT (P60, $n = 3$), CD (P27, $n = 3$), and GC animals treated with rAAV9*hAspA* and rAAV9*hAspA-miRBS* (P60 and P365, $n = 3$). CD brains exhibited widespread high signal intensities, indicating water accumulation particularly in the thalamus (mainly midbrain) and brainstem (**Figure 3c**), which mirror conditions in patients;[27] but T2-weighted hyperintensity in both groups of GC mice was generally reduced (**Figure 3c**). More importantly, reduction of edema seemed to be sustained in P0-treated GC mice for 1 year (**Figure 3c**); however, NAA levels in rAAV9*hAspA*-treated mice were lower than in rAAV9*hAspA-miRBS*–injected mice (**Figure 3d**). Thus, single rAAV injections were able to partially, but sustainably, relieve cerebral edema.
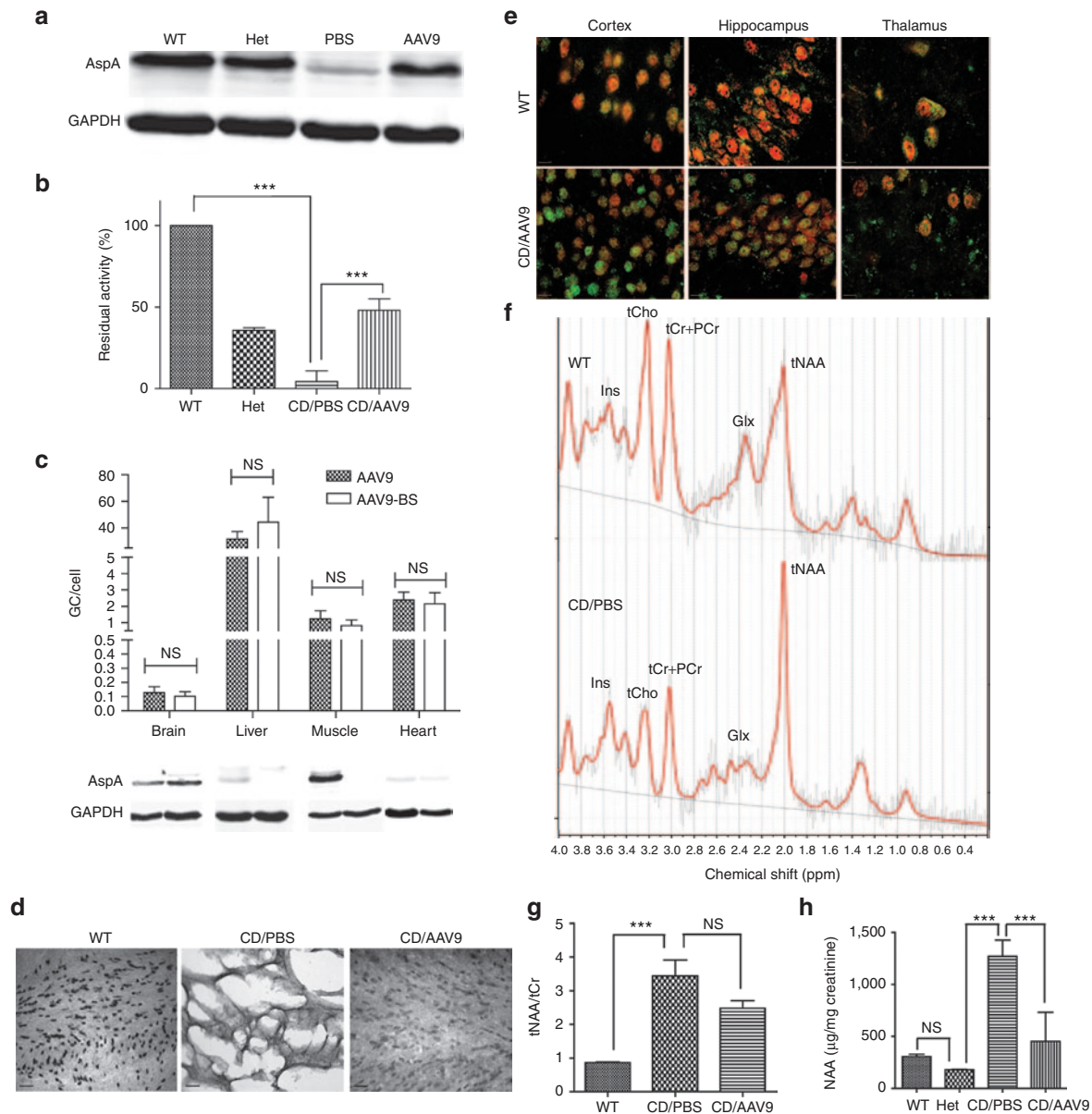
Retinal responses of GC mice were similar to those of age-matched WT mice even after 1 year, although amplitudes of both a- and b-waves were lower, suggesting partial but sustained correction of visual acuities (**Figure 3e**).

Systemic and CNS-restricted *AspA* gene therapy by different rAAVs is therapeutic for CD mice

In addition to rAAV9, two other rAAVs (*i.e.,* rAAVrh.8 and rh.10) were selected for this proof-of-concept gene therapy study in CD mice. Therapeutic efficacies of these vectors (*i.e.,* rAAV9*hAspA*, rAAV9*hAspA-miRBS*, rAAVrh.8*hAspA* or rAAVrh.10*hAspA*) were evaluated in CD mice by comparison of growth, survival and negative geotaxis (all four vectors) as well as other motor functions (rAAV9*hAspA* and *rAAV9hAspA-miRBS* only) (**Supplementary Table S2**). All these vectors were delivered IV at P0.

Growth profiling showed that CD mice were phenotypically similar to WT littermates until P13 after which they steadily lost weight until their death (**Figure 4a**, inset). They became emaciated, dehydrated and had difficulties in movement (**Suppplementary Video S1**); however, P0 treatment significantly improved their motor abilities (**Suppplementary Videos S2,S3**). Compared with rAAV9, GC mice treated with different vectors showed no significant differences in survival or growth (**Figure 4a**).
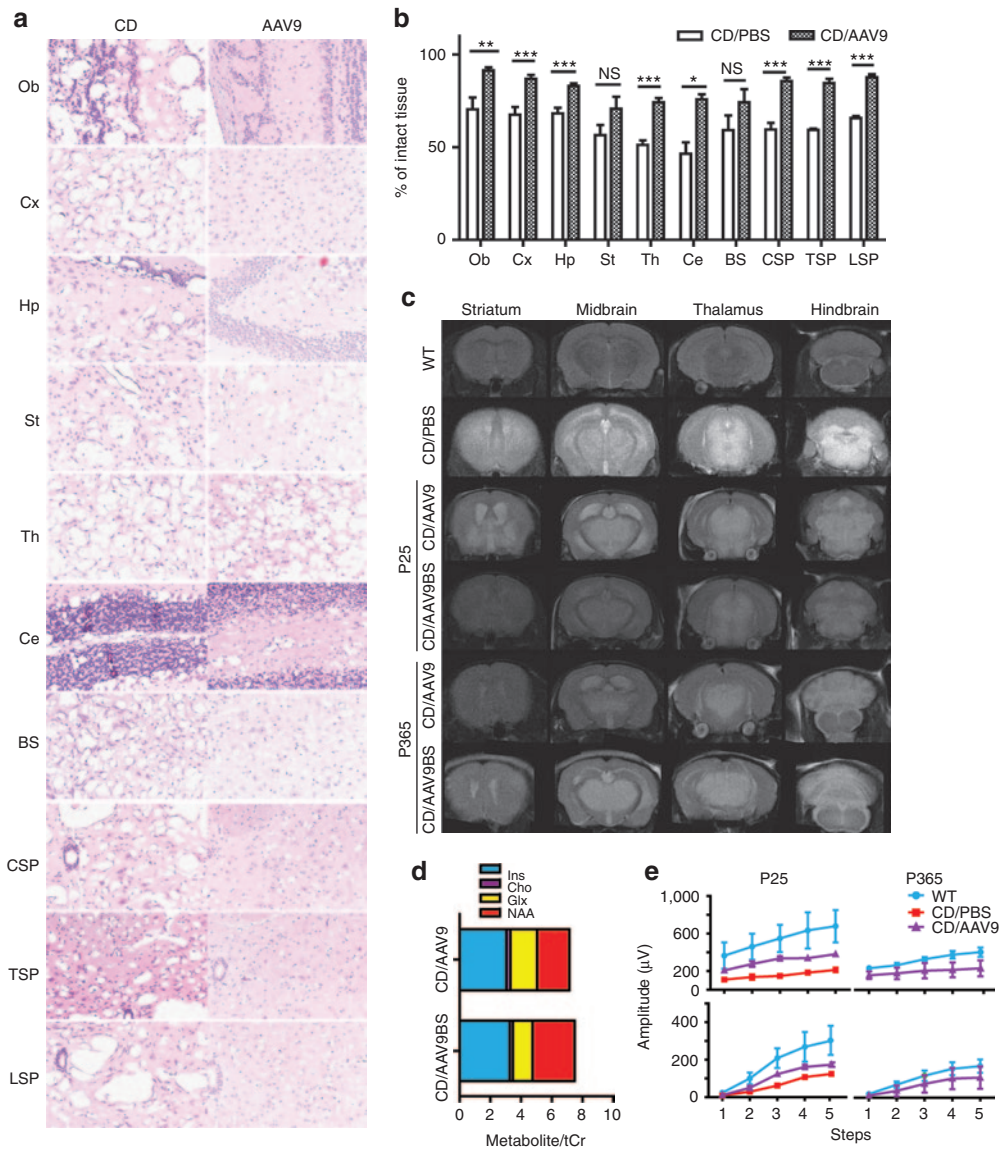
As one of the most important criteria to measure therapeutic benefits of a clinical intervention, survival of >50 GC mice was examined using the Kaplan–Meier curve (**Figure 4b**). There was a uniform rescue of lethality with extended survival as long as 2 years for rAAV9- and rAAVrh.8-injected animals. Long-term study of rAAVrh.10 was initiated about 1 year later; the animals have survived well for 11 months thus far. The negative geotaxis test for early postnatal spatial locomotive behavior showed that

Figure 2 Enzymatic and metabolic correction of AspA deficiency by systemically delivered rAAV-mediated gene therapy in CD mice. (**a**) Western blot of brain homogenates from WT (P90), Het (P90), and CD mice treated with PBS (P27) or rAAV*hAspA* (P90). Loading control: GAPDH. (**b**) Aspartoacylase activity in brain homogenates of the study groups. (**c**) Persistent vector genomes (by quantitative PCR) and aspartoacylase expression (by western blot) in P90 CD/rAAV9hAspA and CD/rAAV9*hAspAmiRBS*. (**d**) Representative images of avidin-biotin-complex (ABC) stained brain sections. (**e**) Immunofluorescence images of brain sections from P90 WT and CD/rAAV9 for AspA (green) and neuronal marker, NeuN (red) and colocalization (yellow). Bars: 10 μm. (**f**) Representative MRS spectra of brain NAA levels in WT and CD/PBS mice at P26 (*n* = 3 each) showing NAA peaks at 2.018 ppm. (**g**) Quantification of *in vivo* brain metabolite levels from the proton spectra as ratio to total creatine. Ins: inositol, tCho: total choline, tNAA: total NAA, tCr: total creatine, Glx: glutamate + glutamine. (**h**) Mass spectrometry of urine from P27 WT, Het and CD/PBS or CD/rAAV9 mice. WT, wild-type; Het, heterozygote; CD/PBS, CD/rAAV9, CD mice treated with PBS or rAAV9 respectively. CD, Canavan's disease; MRS, magnetic resonance spectroscopy; NAA, N-acetyl aspartic acid; NS, not significant; PBS, phosphate-buffered saline; rAAV, recombinant adeno-associated virus.

GC mice but not CD mice performed similar to their WT littermates (**Figure 4c**). CD/rAAV9 mice were compared with CD/phosphate-buffered saline (PBS) mice at P27 and WT at P27, P90, and P180 to further evaluate motor functions. GC mice significantly improved in balance ($P < 0.001$) (**Figure 4d**), and grip ($P < 0.001$) (**Figure 4e**) over CD mice at P27. Data from later timepoints revealed that the treatment fully and sustainably restored grip strength but not balancing abilities in GC mice (**Figure 4d,e**).

GC animals performed significantly better than CD mice on the rotarod at P27 (**Figure 4f,g**) but were significantly behind WT mice at later timepoints (**Figure 4f,g**). The GC mice that received the miRNA-regulated vector performed similar to rAAV9*hAspA*-treated mice in the fixed speed rotarod test but not in balance ($P < 0.001$), inverted screen ($P < 0.05$) and accelerated rotarod ($P < 0.01$) tests at P90 (**Figure 4h**). The GC mice moved like WT mice initially (**Supplementary Videos S2,S3**) but gradually developed

Figure 3 Intravenous (IV) gene therapy using rAAV9 mitigates neuropathology, reduces water accumulation in the brain and improves visual acuity. (**a**) Representative images from hematoxylin and eosin (H&E) stained paraffin sections ($n = 4$ for each group). (**b**) Quantification of neuropathology by ImageJ. Ob, olfactory bulb; Cx, cortex; Hp, hippocampus; St, striatum; Th, thalamus; Ce, cerebellum; BS, brain stem; CSP cervical spinal cord; TSP, thoracic spinal cord; LSP, lumbar spinal cord. (**c**) Representative T2-weighted magnetic resonance imaging images showing water accumulation (white) in P25, CD/PBS; P60, P365 GC; and WT animals. (**d**) Quantification of MRS data for metabolites in brains of mice injected with rAAV9 or rAAV9BS at P0 at age P90. (**e**) Scotopic ERG of WT, CD/PBS and CD/rAAV9 at P25 and P365, respectively, to test visual acuity. WT, wild-type; CD/PBS, CD/rAAV9, CD mice treated with PBS or rAAV9 respectively. CD, Canavan's disease; ERG, electroretinography; MRS, magnetic resonance spectroscopy; NS, not significant; PBS, phosphate-buffered saline; rAAV, recombinant adeno-associated virus.

hind limb paralysis (**Supplementary Video S4**). Overall, our data suggest that IV gene therapy can largely restore motor functions of CD mice.
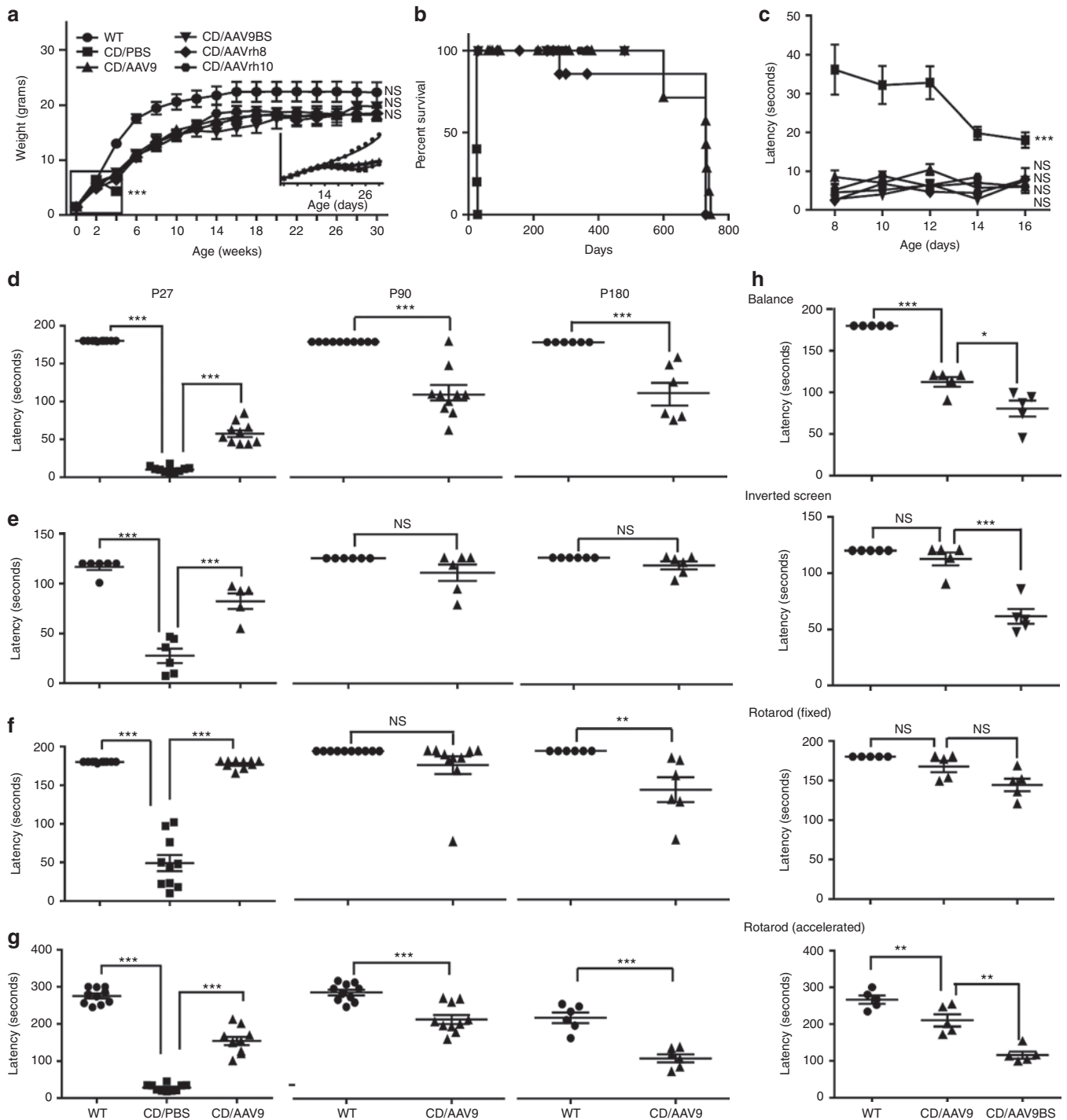
rAAV-mediated intravascular *AspA* gene delivery to the CNS as late as P20 is therapeutic

To define a therapeutic window, CD mice were systemically injected with only rAAV9*hAspA* at P0, P6, P13, and P20 ($n = 6$ each). IV injections at all the timepoints resulted in 100% rescue of early lethality, extended survival (**Figure 5a**) and improved growth profiles (**Figure 5b,c**). Tests for negative geotaxis (**Figure 5d**), balance (**Figure 5e**), grip strength (**Figure 5f**), and abilities

to stay on the rotarod (**Figure 5g,h**) at P90 clearly showed that early intervention was more beneficial to the diseased animals, although injections as late as P20 were sufficient to completely rescue early lethality and partially restore growth and mobility (**Figure 5**, **Supplementary Video S5**).

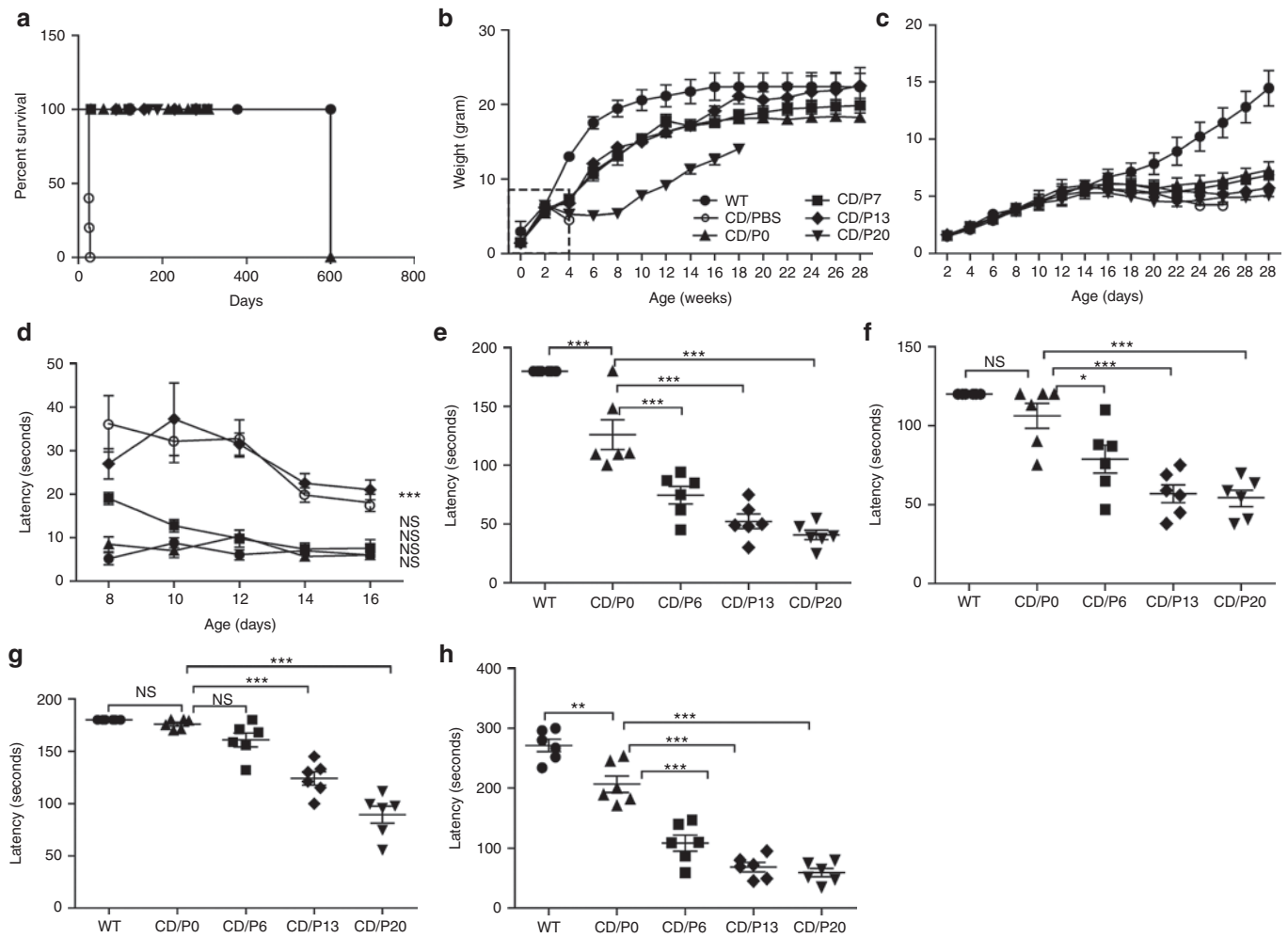## Hypomyelination and abnormal brain lipid profiles are improved by IV gene therapy

Electron microscopy on the brain cortices of P25 mice ($n = 3$ each) showed demyelination around neurons in CD/PBS mice.[4,28] In contrast, the myelin sheaths in GC mice were similar to those of WT in most of analyzed regions (**Figure 6a**). A highly reliable structural

Figure 4 Intravenous (IV) gene therapy using novel rAAVs improves growth profile, rescues early lethality and corrects motor function defects of CD mice. (**a**) Weight of animals at 2-week intervals plotted as a function of time. Early growth rate was assessed by weights at 2-day intervals for the first month (inset). (**b**) Kaplan–Meier survival curves for groups treated with different vectors at P0 ("closed circles" = WT, "closed squares" = CD/PBS, "closed triangles" = CD/rAAV9, "closed up-side down triangles" = CD/rAAV9mirBS, "closed diamonds" = CD/rAAVrh.8, and "closed hexagon" = CD/rAAVrh.10, respectively). (**c**) Negative geotaxis test at intervals of 1 day from P7 (day 8) to P17 (day 16). Motor functions of study groups were tested at P27, P90, and P180 based on their performance on the (**d**) balance beam, (**e**) inverted screen and rotarod moving at (**f**) fixed speed (3 rpm) and (**g**) accelerated speed (4–40 rpm in 5 minutes). The same tests were performed on (**h**) P90 CD/rAAV9 and CD/rAAV9mirBS. WT, wild-type; CD/PBS, CD/rAAV9, CD/rAAV9mirBS, CD/rAAVrh.8, and CD/rAAVrh.10: CD mice treated with PBS, rAAV9*hAspA*, rAAV9*hAspA-mirBS*, rAAVrh.8*hAspA*, and rAAVrh.10*hAspA* at P0, respectively. CD, Canavan's disease; NS, not significant; PBS, phosphate-buffered saline; rAAV, recombinant adeno-associated virus.

index of optimal myelination is the ratio of inner axonal diameter to the outer diameter of the myelin sheath known as the g-ratio.[29] A higher ratio indicates less myelin and altered conduction

capabilities. A semiquantitative comparison of the g ratios between mouse groups further supports the crucial role of AspA in maintaining axonal integrity and myelination (**Figure 6b**).
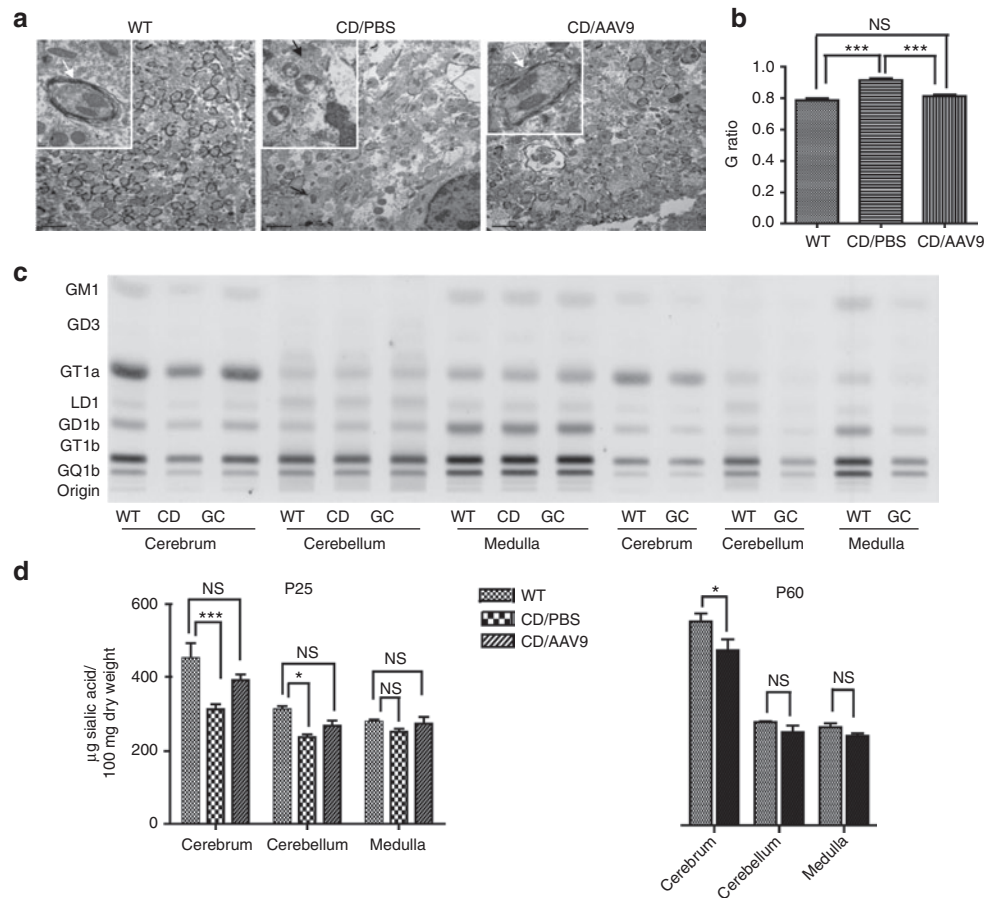
Figure 5 Intravenous (IV) gene therapy with rAAVs as late as P20 improves growth profile, rescues early lethality and corrects motor function defects of CD mice. (**a**) Kaplan–Meier survival curves for all groups treated with different vectors at P0. (**b**) Weight of animals at 2-week intervals plotted as a function of time. (**c**) Early growth rate assessed by weights at 2-day intervals for the first month. (**d**) Negative geotaxis test at intervals of 1 day from P7 (day 8) to P17 (day 16). Motor functions of study groups were tested at P90 based on their performance on the (**e**) balance beam, (**f**) inverted screen and rotarod moving at (**g**) fixed speed (3 rpm) and (**h**) accelerated speed (4–40 rpm in 5 minutes). WT, wild-type; CD/PBS, CD/ P0, CD/P6, CD/P13, and CD/P20: CD mice treated with PBS and rAAV9*hAspA* at P0, P6, P13 and P20 respectively. CD, Canavan's disease; NS, not significant; PBS, phosphate-buffered saline; rAAV, recombinant adeno-associated virus.

Neurochemistry in CD and GC mice was studied by quantitative high-performance thin-layer chromatography (HPTLC) on 21 brain lipids in the cerebrum, cerebellum and medulla collected from WT (P25 and P60), CD (P25 only), and GC (treated at P0, analyzed at P25 and P60) mice ($n = 3$ each). Compared with WT mice, at P25, the total concentration of gangliosides was lower in the cerebrum and cerebellum of CD mice whereas gene therapy largely corrected this defect (**Figure 6c,d**). Concentrations of neuronal-enriched gangliosides (GD1a, GT1b, and GQ1b) at P25 were significantly lower in CD mice than the WT mice but were largely corrected in the GC mice (**Figure 6c**, **Supplementary Table S1**). Although the concentrations of all major gangliosides were lower in the GC mice compared with WT mice, none of these reductions was significant except for GM1 in the cerebrum (**Supplementary Table S1**). CD mice had significantly lower cholesterol content in the cerebrum and medulla compared with WT mice. Though largely corrected in the GC mice at P25, significant reduction was still seen in

the cerebrum and cerebellum of GC mice at P60 (**Figure 6c**, **Supplementary Table S1**).

It is noteworthy that deficiencies in cerebrosides and sulfatides were not completely corrected in the GC mice at either age (**Table 1**). Cerebrosides and sulfatides migrate as double bands on the HPTLC due to differences in their hydroxyl fatty acid content (**Supplementary Figure S1a,b**).[30] The slower (lower, L) migrating band mostly contains short-chain hydroxylated fatty acids; whereas, the faster (upper, U) band mostly contains longer chain non-hydroxylated fatty acids.[30] Based on our HPTLC data (**Table 1**), it appears that the increased L/U (lower/upper band) ratio in the CD and GC mice is due to a greater deficiency of the non-hydroxylated fatty acids.

Myelin structure in optic nerves and spinal cords from WT ($n = 4$), CD/PBS ($n = 5$), and CD/rAAV9 mice at P26 ($n = 4$) (**Supplementary Figure S2**) was examined using X-ray diffraction to quantify structural parameters like myelin period and relative amount of myelin.[31,32] Diffraction from both tissues yielded strong

Figure 6 Intravenous (IV) gene therapy using rAAV9 improves myelin synthesis and partially corrects lipid profile of myelin in CD mice.
(**a**) Electron microscopy of the motor cortex of P27 age-matched mice ($n = 3$ for each cohort). Bar: 2 μm. Inset: higher magnification. Black arrows: unmyelinated axons; white arrows: myelin sheath. (**b**) G ratios of myelinated axons calculated from toluidine blue stained sections of the cortex using ImageJ. (**c**) High-performance thin-layer chromatography of gangliosides in cerebrum, cerebellum, and medulla of different mouse groups ($n = 3$ for each group). Lower panel: quantification of the plate. (**d**) Quantification of the high-performance thin-layer chromatography plate. Canavan's disease; GC, gene-corrected mice; NS, not significant; PBS, phosphate-buffered saline; rAAV, recombinant adeno-associated virus.

intensity maxima, indicating the presence of significant amounts of multilamellar myelin (**Supplementary Figure S2a,b**). Each group displayed similar relative amounts of myelin (**Supplementary Figure S2c,d**). Myelin period is defined as the distance between subsequent pairs of bilayers. Any aberration in periodicity indicates inadequate insulation and subsequent neurological impairment. Spinal cords from CD/rAAV9 mice displayed a significantly higher myelin period (160.3 ± 0.5 Å) ($P < 0.04$) compared with CD/PBS mice (159.1 ± 0.8 Å). Optic nerves, CD/rAAV9 samples had a significantly higher period (157.7 ± 0.7 Å) than WT (156.6 ± 0.7 Å) ($P < 0.006$) (**Supplementary Figure S2c,d**). Other differences in myelin period and amount were not statistically significant. The I_2/I_4 ratio is a measure of the relative intensity of the 2nd order X-ray reflection over the 4th order reflections. Comparison of the I_2/I_4 ratios revealed a statistically significant decrease in the CD/rAAV9 mice compared with WT (**Supplementary Figure S2e,f**), indicating a small change in membrane structure.

DISCUSSION
Our study aims to develop efficacious therapeutics for CD using the $AspA^{-/-}$ KO mouse model and systemically delivered rAAVs for CNS-targeted $AspA$ gene therapy as well as address off-target

transgene expression in peripheral tissues. The $AspA^{-/-}$ mouse model in SV129/Ev background 10 recapitulates the severest form of CD. Animals show progressive neuropathy and retinopathy, severe developmental delay, difficulties in mobility and whole body tremors around P19, which gradually worsens until their death around P27 (**Figures 1** and **4a**, **Supplementary Video S1**) making them a stringent preclinical model to study the molecular etiology of AspA deficiency and evaluate efficacious therapeutics, primarily based on the rescue of early lethality. Our study clearly demonstrated the feasibility of completely rescuing the early lethality, slowing down the disease progression, and extending the survival of CD mice (**Figure 4b**, **Supplementary Video S3**). Our findings address several critical issues in systemically delivered CNS gene therapy. First, IV injections of rAAVrh.8 and rAAVrh.10 to CD mice at P0 are therapeutically equivalent to rAAV9, significantly improving their early motor function and growth, and effectively rescuing early lethality, which expands options in the existing rAAV repertoire to select serologically suitable vectors for patient populations (**Supplementary Table S2**). Our data also provide the first evidence of harnessing endogenous miRNA to regulate therapeutic expression of rAAV tissue specifically, which is shown to be safe, not disturbing homeostasis or function of endogenous

Table 1 Molecular species composition of cerebrosides and sulfatides in normal (WT) Canavan's disease (CD) and CD mice treated with AAV gene therapy (GC)

| Age | Brain region | Genotype | L/U ratio[a] | |
			Cerebrosides	Sulfatides
25 days	Cerebrum	WT	2.23 ± 0.11	0.74 ± 0.07
		CD	4.95 ± 0.73*	1.06 ± 0.06*
		GC	7.87 ± 0.29**	1.12 ± 0.06*
	Cerebellum	WT	1.22 ± 0.03	0.38 ± 0.03
		CD	2.09 ± 0.24*	0.40 ± 0.08
		GC	1.98 ± 0.13*	0.37 ± 0.02
	Medulla	WT	1.38 ± 0.07	0.63 ± 0.02
		CD	1.53 ± 0.07	0.74 ± 0.02**
		GC	1.50 ± 0.08	0.81 ± 0.01**
60 days	Cerebrum	WT	2.07 ± 0.01	0.56 ± 0.07
		GC	4.47 ± 0.70*	0.85 ± 0.20
	Cerebellum	WT	1.47 ± 0.03	0.48 ± 0.03
		GC	2.47 ± 0.29	0.76 ± 0.10
	Medulla	WT	1.39 ± 0.07	0.49 ± 0.01
		GC	2.21 ± 0.21*	0.71 ± 0.04*

Abbreviations: AAV, adeno-associated virus; GC, gene-corrected mice; L/U ratio, lower (L)/upper (U) band ratio; WT, wild-type.
[a]Values represent ratio of the lower band (hydroxy fatty acids) to the upper band (non-hydroxy fatty acid) $\pm$ SE ($n = 3$ independent samples per group). Determined from densitometric scanning of high-performance thin-layer chromatography plates.
Significant difference from the WT mice at *$P < 0.05$, **$P < 0.01$ as determined by the unpaired two-tailed t-test.

miRNAs.[23] In addition, the success of IV gene therapy as late as P20 in CD mice represent a clinically relevant advance from the documented therapeutic benefit at P10 in a mouse model for spinal muscular atrophy.[33] However, we did observe reduced mobility in the later treated animals (**Figure 4d–g**), which indicates that early intervention is therapeutically more beneficial, echoing the results of a recently concluded CD gene therapy study on patients.[20]

Robust neuronal transduction in GC mice (**Figure 2e**) suggested that rAAV9 delivered AspA may improve myelin structures by hydrolyzing NAA at its source but may not help myelination by oligodendrocytes. Our detection of AspA-expressing neurons in the WT animals also differs from published data[34–37] but would explain the widespread activity detected in cerebral hemispheres (**Figure 2d**), although we cannot discount possible cross-reactivity of our AspA antibody with amidohydrolase I[38,39] that has only 7% reactivity[40] toward NAA.

Improved motor functions (**Figures 4d–h** and **5e–h**) might result from reconstituted AspA and mitigated neuropathology in the pyramidal nuclei of the hindbrain and spinal cord of treated mice (**Figure 3a,b**). However, we did see partial hind limb paralyses with dragging of hind limbs and decline in mobility starting around 8 months postinjection (**Supplementary Video S4**), although the animals still have intact righting reflexes, move around and eat with no obvious weight losses. One possible cause for the late-onset motor dysfunctions could be due to a gradual loss of rAAV-mediated AspA expression as a consequence of glial cell transduction and regeneration. Around 14 months, the animals started showing infrequent and brief seizures. Readministration of serologically different rAAVs by a different route may help to sustain correction of myelin neurochemistry and motor function

as CNS-directed rAAV gene transfer by intracerebroventricular injections is assessable for readministration.[41]

Lipid abnormalities for myelin-enriched cerebrosides in CD mice were largely similar to those in the tremor rat model of CD.[42] Since cholesterol is a major component of the myelin sheath, its reduction can be attributed to defects in myelin content.[43] CNS-targeted AspA gene transfer by rAAVs appears to correct abnormalities in ganglioside and cholesterol levels but not the myelin-specific (cerebrosides) or myelin-enriched (sulfatides and GM1 ganglioside) lipids (**Figure 6d**, **Table 1**). The subtle differences in electron density distribution within the myelin sheath detected among all groups (**Supplementary Figure S2**), are also consistent with altered lipid profiles. Further studies are warranted to compare the physiochemical properties and biophysical structures of myelin in the CD and GC mice. X-ray diffraction analysis, however, did not detect differences in relative amount of myelin between WT, CD, and GC mice. It is unclear whether this is a result of changes in axon diameter, lower total scatter from affected animals or region-specific differences in optic nerves and spinal cords. In addition, the dramatic loss of vision in CD mice (**Figure 1c**) might arise from demyelination of optic nerves, retinal degeneration, and pathological changes in cell types responsible for visual acuity, or all of the above.

When translated into human applications, the vector dose regimen used in our study is $\sim 4 \times 10^{14}$ vector genomes/kg. Even though similar doses have recently been approved for systemic delivery of rAAV9 to pediatric patients of spinal muscular atrophy;[44] lower doses would reflect a more favorable risk-to-benefit ratio clinically and reduced vector manufacturing burden. Hence, for the next phase of our CD gene therapy study, we planned for a dose down-escalation study to identify the minimum effective dose.

In conclusion, our study demonstrates the crucial role of AspA in myelination and early neurodevelopment as well as the feasibility of treating CD by CNS-targeted gene therapy using systemically delivered rAAVs. While more studies such as addressing potential role(s) of NAA in energetics of the CNS are necessary to further elucidate pathophysiology of AspA deficiency, a more comprehensive comparison of three leading vectors (*i.e.,* rAAV9, rAAVrh.8 and rAAVrh.10) in CD mice may be warranted to select a clinical candidate vector. Afterwards, a formal toxicology, safety and biodistribution study of the clinical candidate vector in nonhuman primates may constitute a critical path leading to human clinical applications for gene therapy of CD and other untreatable CNS diseases.

MATERIALS AND METHODS

Viral production. The recombinant vector genome contains AAV2 inverted terminal repeats that flank the human cytomegalovirus-enhancer/chicken β-actin promoter, human AspA cDNA, and rabbit globin poly(A) sequences, totaling ~ 2.1 kb. For the miRNA-regulated vector genome, three copies each of target sequences of miR-1 and miR-122 were cloned in tandem into the 3′ untranslated region of *AspA* cDNA as described previously.[23] The plasmid was sequenced throughout the expression cassette, and integrity of the inverted terminal repeats was confirmed by restriction analysis. Before being packaged with different AAV capsids, functionality of the construct was verified by *in vitro* transfection in 293 cells and measurement of AspA enzyme activity.

All rAAV vectors were produced by transient transfection of 293 cells and CsCl gradient sedimentation as previously described[45] Vector preparations were titered by quantitative PCR, purity of vectors was assessed by 4–12%

SDS-acrylamide gel electrophoresis and silver staining (Invitrogen, Carlsbad, CA) and morphological integrity of virions was assessed by transmission electron microscopy of negative stained recombinant AAV virions at Electron Microscopy Core, UMass Medical School, Worcester, MA.

Animal procedures. All animal procedures were approved by the Institutional Animal Care and Use Committee of UMass Medical School. AspA$^{+/-}$ Sv129/Ev mice littermates were bred using programmatic timing and newborn pups were dosed on P0. Vectors were injected in the facial vein of P0 pups at doses of 4×10^{11} GC/mouse. P6, P13, and P20 pups were injected in the retro-orbital sinus with 8×10^{11}, 1.2×10^{12}, and 4×10^{12} GC/mouse, respectively. After the injection pups were cleaned, rubbed with bedding, and then returned to their cage. The dam was reintroduced after brief nose numbing using ethanol pads.

Immunohistochemistry. Animals were anesthetized, transcardially perfused with 4% paraformaldehyde (vol/vol) in PBS. Whole carcasses were postfixed in fixative for 1 day. Organs were extracted, rinsed in PBS, and sagitally sectioned. One half was cryoprotected in 30% sucrose (wt/vol) in PBS at 4 °C, embedded in OCT compound (Sakura Finetek, Torrance, CA) and frozen in a dry ice/ethanol bath; 40 μm floating sections of the entire brain were cut in a Cryostat (Thermo Microm HM 550; Thermo Fisher Scientific, Kalamazoo, MI) for immunostaining. The other half was processed for hematoxylin and eosin staining for morphological studies.

Floating sections were stained in 12-well plates. Sections were washed once in PBS for 5 minutes, and incubated in blocking solution containing 0.05% Tween-20 (vol/vol) (Fisher, Pittsburgh, PA), and 10% goat serum (vol/vol) (Invitrogen) for 1 hour at room temperature. Sections were incubated with primary antibodies at 4 °C overnight, washed twice in 0.05% Tween-20 in PBS (PBST) for 15 minutes each followed by incubation in appropriate secondary antibodies at room temperature for 1 hour. Sections were washed twice in PBST for 10 minutes each before mounting on glass slides. Vectashield with 4′,6-diamidino-2-phenylindole (Vector Laboratories, Burlingame, CA) was used to mount all slides. Omission of either the primary or the secondary antibody in single-label experiments resulted in no labeling.

The ABC stain was performed according to standard kit instructions (Elite ABC kit; Vectastain, Burlingame, CA). DAB was used as the substrate for the peroxidase enzyme reaction (Vectastain).

The primary antibodies used were as follows: mouse monoclonal antibodies to human aspartoacylase (Abmart, Shanghai, China), rabbit aspartoacylase (provided by Dr Aryan Namboodiri); mouse NeuN (MAB-377, clone A60; Millipore, Billerica, MA); rabbit NeuN (ABN-78; Millipore) and appropriate secondary antibodies from Invitrogen.

Imaging and image analysis. Stained sections were examined using DM 5500B Upright microscope (Leica Microsystems, Wetzlar, Germany), and images were captured with Leica DFC365 FX high-sensitivity monochrome digital camera. Regions of interest were identified according to the mouse brain atlas. Z stack of images were taken with a 63X objective and ×1.6 additional magnification for each channel and overlaid to obtain a multicolor image at ×100.8. Deconvolution was performed using Leica Application Suite Advanced Fluorescence software.

ERG. Mice were dark adapted overnight and anesthetized with 100 mg/kg ketamine and 20 mg/kg xylazine in saline before testing. Both pupils were topically dilated with phenylephrine hydrochloride and 1% tropicamide, and mice were placed on a heated platform. Rod-dominated responses were elicited in the dark with 10 μs flashes of white light (1.37×105 cd m^{-2}) presented at intervals of 1 minute in a Ganzfeld dome. ERGs were monitored simultaneously from both eyes with a silver wire loop electrode in contact with each cornea wetted with celluvisc containing carboxymethylcellulose sodium 1%.

Western blot. Mice were killed and their tissues were extracted and homogenized as described.[23] Protein in equal quantities was loaded into a 12%

Tris-HCl gel well (Bio-Rad Laboratories, Hercules, CA) and transferred to a nitrocellulose membrane (Bio-Rad). The membrane was incubated in blocking buffer for 1 hour followed by AspA polyclonal antibody overnight. After three washes in 0.1% PBST, it was incubated with secondary antibodies conjugated to LI-COR IRDye for 1 hour at room temperature. After two washes with 0.1% PBST, signal was detected using the Odyssey Imager (LI-COR Biosciences, Lincoln, NE).

Genome copy number. rAAV genomes were quantified in 1 μg of genomic DNA extracted from mouse tissues using the QIAamp DNA mini kit for quantitative detection of vector genome copies by Taqman probes ((Applied Biosystems, Foster City, CA) with a single-copy endogenous GAPDH gene) as the diploid cell number reference. The Taqman real-time PCR kit was run with primer sets which amplified regions of the nRBG poly A (Probe, 6FAM-ATG AAG CCC CTT GAG CAT CTG ACT TCT-TAMRA; forward, GCC AAA AAT TAT GGG GAC AT; reverse, ATT CCA ACA CAC TAT TGC AAT G). The sensitivity of the assay was 10 copies/150 ng of cellular DNA.

AspA activity assay. Mice were killed 3 months after injection, and brain homogenates were used for the enzyme assay.[10] Briefly, the brain was homogenized and incubated with 50 mmol/l Tris-HCl (pH 8.0), 0.5% (wt/vol) NP-40, 50 mmol/l NaCl, 1 mmol/l CaCl$_2$, 2.8 mmol/l NAA in a total volume of 600 μl. After incubation at 37 °C for 3 hours, the assay mixture was centrifuged and the supernatant was incubated with malic dehydrogenase, glutamic oxalacetic transaminase, and NADH for 10 minutes at 37° C. The amount of L-aspartate released was estimated by decrease in absorbance due to the conversion of NADH to NAD using a spectrophotometer (Shimadzu, Columbia, MD) at 340 nm. One milliunit of aspartoacylase activity is equivalent to 1 nmol of aspartate released in 1 minute. Values were calculated using analysis of variance. The value $P < 0.05$ was considered significant.

¹H magnetic resonance imaging and spectroscopy study. Mice were anesthetized with 2% isofluorane and constantly monitored for vital signs. All imaging experiments were performed using a 4.7T/40 cm horizontal magnet (Oxford, UK) equipped with a Biospec Bruker console (Bruker, Germany). A ¹H radiofrequency coil configuration (Insight NeuroImaging Systems, Worcester, MA) with inner diameter of 4 cm was used for the experiments.

T2-weighted anatomical images were acquired using a fast spin-echo sequence (RARE) (repetition time = 3,000 ms, echo time = 48 ms, matrix size = 256×256, field of view = 2.5×2.5 cm, slice number = 16, slice thickness = 1 mm). ¹H magnetic resonance spectroscopy data were acquired using single voxel (Pont Resolved Spectroscopy Sequence) (repetition time = 2,500 ms, echo time = 20 ms, N average = 1,024, voxel size = 3×3×3 mm).

Proton spectra were fit using LCModel (Version 6.2-2B) which analyzed *in vivo* proton spectrum as a linear combination of model *in vitro* spectra from individual metabolite solutions (Provencher, 2001) and generated data as absolute fits (in institutional units) and SD%. SD was used as a measure of the reliability of the fit. The spectral inclusion criteria were SD <20% for NAA, creatine, and inositol.

Behavioral studies. Negative geotaxis test was performed on P7–P17 pups where they were placed on a 45° inclined plane; head facing downwards and their latency to turn with the head pointing upwards was recorded.

For the beam balance test, animals were placed in the middle of a horizontal wooden balance beam (1.5 × 100 cm) with pads underneath to protect mice that might fall off the beam. Latency to fall was recorded, with a 3 minutes time limit for each trial.

Neuromuscular function of the mice was assessed by testing grip strength on an inverted screen. Mice were placed in the center of a screen (30 cm² square-wire mesh, 25 mm² holes) until they gripped the mesh. The screen was then inverted above a cushioned surface for a 2 seconds

period with the mouse's head declining. Latency to fall from the screen was recorded, with a 2-minute time limit for each trial.

Mice were subjected to a rotarod test to evaluate motor coordination and balance. Each animal was placed on the rotarod after which speed was adjusted to 3 rpm. The latency to fall off the rotarod within this time period was recorded for fixed speed. Animals were also tested for their latency to fall off at accelerated speeds going from 4 to 40 rpm in 5 minutes. Animals were tested for each experiment three times with an intertrial interval of ~30 minutes for each animal and mean of three trials was used to plot the graphs.

Transmission electron microscopy. Mice were anesthetized and perfused with a solution of 2.5% glutaraldehyde in 0.05 mol/l sodium phosphate buffer, pH 7.2. The brain was extracted and incubated in 2.5% glutaraldehyde in 0.05 mol/l Cacodylate buffer overnight at 4 °C. It was sectioned into 1 mm thick sections, rinsed twice in the same buffer and postfixed with 1% osmium tetroxide for 1 hour at room temperature. Sections were washed in DH_2O for 20 minutes at 4 °C and then dehydrated in graded ethanol series of 20% increments, before two changes in 100% ethanol. Sections were infiltrated with two changes of 100% propylene oxide and then with a 50%/50% propylene oxide/SPI-Pon 812 resin mixture overnight. After three changes of fresh 100% SPI-Pon 812 resin, sections were polymerized at 68 °C in plastic capsules. Regions of interest were cut out and thick-sectioned for toluidine blue. Chosen regions were reoriented and ~70 nm thin sections were placed on copper support grids and contrasted with lead citrate and uranyl acetate. Sections were examined using the FEI Tecani 12 BT with 80 kV accelerating voltage, and images were captured using a Gatan TEM CCD camera.

Total lipid isolation. Total brain lipids were evaluated from the frozen cerebrum, cerebellum, and medulla of P25 and P60 WT, CD/PBS, and CD/rAAV9 mice. Tissues were homogenized in water and lyophilized for 24 hours. After desiccation, the dried tissue was weighed, rehydrated in water (0.05 ml), and lipids were extracted overnight in $CHCl_3:CH_3OH$ (1:1; vol/vol) according to standard procedures.[30] Lipids were further separated into a neutral (F1) and acidic/ganglioside (F2) fraction *via* ion exchange chromatography over a Sephadex column. Neutral lipids and cholesterol were eluted with a $CHCl_3:CH_3OH:dH_2O$ (30:60:8; vol/vol/vol) solution, while acidic phospholipids and gangliosides were eluted with a $CHCl_3:CH_3OH:0.8$ mol/l $C_2H_3NaO_2$ (30:60:8; vol/vol/vol) solution. Gangliosides were separated from acidic phospholipids by Folch partitioning, base treated, and desalted. Neutral lipids were dried by rotary evaporation and resuspended in 10 ml $CHCl_3:CH_3OH$ (2:1; vol/vol).

Sialic acid quantification. Total ganglioside content was quantified before and after desalting using the resorcinol assay. Three aliquots of each ganglioside sample were dried under vacuum. Resorcinol reagent: water (1:1 vol/vol) solution (resorcinol reagent—HCl:0.2 mol/l resorcinol:dH_2O:0.1 mol/l $CuSO_4$, 40:5:5:0.125 vol/vol/vol/vol) was added to each sample, followed by submersion in a boiling water bath for 15 minutes. After cooling on ice, the reaction was stopped with butyl acetate: N-butanol (85:15; vol/vol). Each sample was vortexed and centrifuged at 700*g* for 2 minutes. The absorbance of the upper aqueous layer was recorded at 580 nm using a Shimadzu UV-1601 Spectrophotometer (Shimadzu, Torrance, CA). Sialic Acid values were fit to a standard curve using N-acetylneuraminic acid as a standard.

TLC. All lipids were analyzed by HPTLC as previously described. Neutral and acidic lipids were spotted using a Camag Linomat II auto-TLC spotter (Camag Scientific, Wilmington, NC). The amount of neutral lipid spotted corresponded to 70 μg dry weight. The plate was developed in solvent system I to 4.5 cm which contained C:M:acetic acid:formic acid:H_2O (70:30:12:4:2 by volume) and solvent system II to the top which contain hexane: isopropyl ether: acetic acid (65:35:2 by volume). The amount of acidic lipid spotted corresponded to 200 μg of dry weight and was developed in solvent system I to 6.0 cm and in solvent II to the top. Bands for both neutral lipids and acidic lipids were visualized by charring with 3% cupric acetate in 8% phosphoric acid

solution in an oven at 160 °C for 7 minutes. Gangliosides were spotted based on 1.5 μg of sialic acid and were developed in chloroform:methanol:0.02% calcium chloride (C:M:0.02% $CaCl_2$). Individual lipid bands were scanned using Camag TLC Scanner 4 and the concentration of cerebrosides and sulfatides were calculated from a standard curve.[30] The total brain ganglioside distribution was normalized to 100% and the percentage distribution values were used to calculate sialic acid concentration of GM1.

X-ray diffraction analysis. X-ray diffraction was performed as described.[32] Briefly, optic nerves and spinal cords were dissected from mice killed using isoflurane. Optic nerves and sagitally bisected segments of cervical spinal cord were maintained in physiological saline (154 mmol/l NaCl, 5 mmol/l phosphate, pH 7.4) and loaded into thin-walled, quartz capillary tubes which were then filled with saline and sealed with wax and enamel. X-ray diffraction experiments were carried out using nickel-filtered, single-mirror focused CuKα radiation from a fine-line source on a 3.0 kW Rigaku X-ray generator operated at 40 kV by 10 mA. Exposure times were 30 minutes. Diffraction patterns were collected using a linear, position-sensitive detector (Molecular Metrology, Northampton, MA) and analyzed using PeakFit (Jandel Scientific, San Rafael, CA). Myelin period was calculated from the positions of the intensity maxima in the diffraction patterns. The relative amount of myelin in each sample was calculated by measuring the total integrated intensity of all maxima over background, excluding small-angle scatter around the beam stop and wide-angle scatter.

Statistical analyses. Statistical calculations included log-rank Mantel–Cox test for the survival table and one-way analysis of variance followed by Tukey's multiple comparison test for all other experiments. $^*P < 0.05$; $^{**}P < 0.01$; $^{***}P < 0.001$, NS: not significant.

SUPPLEMENTARY MATERIAL
Figure S1. Comparison of the neurochemistry of brain lipids.
Figure S2. X-ray diffraction analyses of myelin structures.
Table S1. Regional distribution of neutral and acidic lipids in 25-day-old and 60-day-old normal (WT), Canavan's disease (CD), and CD mice treated with AAV gene therapy (GC).
Table S2. Summary chart showing outcomes of different therapeutic approaches with different rAAV serotypes.
Video S1. P27-untreated CD male mouse that is emaciated, dehydrated, and has difficulties in movement.
Video S2. Age-matched untreated CD mouse with a mouse injected at P0 with rAAV9*hAspA* at P27.
Video S3. Two months old WT and CD mouse treated with intravenous injection of rAAV9*hAspA* at P0.
Video S4. Eight months old animals treated with rAAV9*hAspA* at P0.
Video S5. Three months old animals treated with rAAV9*hAspA* at P20.

REFERENCES

1. Van Bogaert, L (1949). Sur une idiotie familiale avec dégénérescence spongieuse de nevraxe. *Acta Neurol Belg* **49**: 572–587.
2. Traeger, EC and Rapin, I (1998). The clinical course of Canavan disease. *Pediatr Neurol* **18**: 207–212.
3. Matalon, RM and Michals-Matalon, K (2000). Spongy degeneration of the brain, Canavan disease: biochemical and molecular findings. *Front Biosci* **5**: D307–D311.
4. Beaudet, A (2001). Aspartoacylase deficiency (Canavan disease). In: Scriver, CR, Beaudet, AL, Sly, WS, Valle, D (eds). *The Metabolic and Molecular Bases of Inherited Disease*. pp. 5799–5805.
5. Matalon, R, Michals, K, Sebesta, D, Deanching, M, Gashkoff, P and Casanova, J (1988). Aspartoacylase deficiency and N-acetylaspartic aciduria in patients with Canavan disease. *Am J Med Genet* **29**: 463–471.
6. Kaul, R, Gao, GP, Balamurugan, K and Matalon, R (1993). Cloning of the human aspartoacylase cDNA and a common missense mutation in Canavan disease. *Nat Genet* **5**: 118–123.
7. Birnbaum, SM, Levintow, L, Kingsley, RB and Greenstein, JP (1952). Specificity of amino acid acylases. *J Biol Chem* **194**: 455–470.
8. Baslow, MH and Resnik, TR (1997). Canavan disease. Analysis of the nature of the metabolic lesions responsible for development of the observed clinical symptoms. *J Mol Neurosci* **9**: 109–125.
9. Kvittingen, EA, Guldal, G, Børsting, S, Skalpe, IO, Stokke, O and Jellum, E (1986). N-acetylaspartic aciduria in a child with a progressive cerebral atrophy. *Clin Chim Acta* **158**: 217–227.
10. Matalon, R, Rady, PL, Platt, KA, Skinner, HB, Quast, MJ, Campbell, GA *et al.* (2000). Knock-out mouse for Canavan disease: a model for gene transfer to the central nervous system. *J Gene Med* **2**: 165–175.
11. Kitada, K, Akimitsu, T, Shigematsu, Y, Kondo, A, Maihara, T, Yokoi, N *et al.* (2000). Accumulation of N-acetyl-L-aspartate in the brain of the tremor rat, a mutant exhibiting absence-like seizure and spongiform degeneration in the central nervous system. *J Neurochem* **74**: 2512–2519.
12. Traka, M, Wollmann, RL, Cerda, SR, Dugas, J, Barres, BA and Popko, B (2008). Nur7 is a nonsense mutation in the mouse aspartoacylase gene that causes spongy degeneration of the CNS. *J Neurosci* **28**: 11537–11549.
13. Mersmann, N, Tkachev, D, Jelinek, R, Röth, PT, Möbius, W, Ruhwedel, T *et al.* (2011). Aspartoacylase-lacZ knockin mice: an engineered model of Canavan disease. *PLoS ONE* **6**: e20336.
14. Gao, G, Vandenberghe, LH and Wilson, JM (2005). New recombinant serotypes of AAV vectors. *Curr Gene Ther* **5**: 285–297.
15. Gao, GP, Alvira, MR, Wang, L, Calcedo, R, Johnston, J and Wilson, JM (2002). Novel adeno-associated viruses from rhesus monkeys as vectors for human gene therapy. *Proc Natl Acad Sci USA* **99**: 11854–11859.
16. Mingozzi, F and High, KA (2011). Immune responses to AAV in clinical trials. *Curr Gene Ther* **11**: 321–330.
17. Asokan, A, Schaffer, DV and Samulski, RJ (2012). The AAV vector toolkit: poised at the clinical crossroads. *Mol Ther* **20**: 699–708.
18. Gao, GS, Weng, PJ, Ji, RB, Li, DZ, Li, YY, Li, HS *et al.* (2010). [Effect of hepatitis B virus X gene on the expression of spastic paraplegia 21]. *Zhonghua Gan Zang Bing Za Zhi* **18**: 920–923.
19. Janson, C, McPhee, S, Bilaniuk, L, Haselgrove, J, Testaiuti, M, Freese, A *et al.* (2002). Clinical protocol. Gene therapy of Canavan disease: AAV-2 vector for neurosurgical delivery of aspartoacylase gene (ASPA) to the human brain. *Hum Gene Ther* **13**: 1391–1412.
20. Leone, P, Shera, D, McPhee, SW, Francis, JS, Kolodny, EH, Bilaniuk, LT *et al.* (2012). Long-term follow-up after gene therapy for canavan disease. *Sci Transl Med* **4**: 165ra163.
21. Foust, KD, Nurre, E, Montgomery, CL, Hernandez, A, Chan, CM and Kaspar, BK (2009). Intravascular AAV9 preferentially targets neonatal neurons and adult astrocytes. *Nat Biotechnol* **27**: 59–65.
22. Zhang, H, Yang, B, Mu, X, Ahmed, SS, Su, Q, He, R *et al.* (2011). Several rAAV vectors efficiently cross the blood-brain barrier and transduce neurons and astrocytes in the neonatal mouse central nervous system. *Mol Ther* **19**: 1440–1448.
23. Xie, J, Xie, Q, Zhang, H, Ameres, SL, Hung, JH, Su, Q *et al.* (2011). MicroRNA-regulated, systemically delivered rAAV9: a step closer to CNS-restricted transgene expression. *Mol Ther* **19**: 526–535.
24. Grodd, W, Krägeloh-Mann, I, Petersen, D, Trefz, FK and Harzer, K (1990). *In vivo* assessment of N-acetylaspartate in brain in spongy degeneration (Canavan's disease) by proton spectroscopy. *Lancet* **336**: 437–438.
25. Pioro, EP, Wang, Y, Moore, JK, Ng, TC, Trapp, BD, Klinkosz, B *et al.* (1998). Neuronal pathology in the wobbler mouse brain revealed by *in vivo* proton magnetic resonance spectroscopy and immunocytochemistry. *Neuroreport* **9**: 3041–3046.
26. Matalon, R, Kaul, R and Michals, K (1993). Canavan disease: biochemical and molecular studies. *J Inherit Metab Dis* **16**: 744–752.
27. Matalon R, Kaul, R and Michals, K (1997). The molecular and genetic basis of neurological disease. In: Rosenberg, RN, Prusiner, SB, Di Mauro, S, Barchi, RL (eds). *Canavan Disease*. Butterworth-Heinemann: Boston, MA. pp. 493–502.
28. Adachi, M, Torii, J, Schneck, L and Volk, BW (1972). Electron microscopic and enzyme histochemical studies of the cerebellum in spongy degeneration (van Bogaert and Bertrans type). *Acta Neuropathol* **20**: 22–31.
29. Chomiak, T and Hu, B (2009). What is the optimal value of the g-ratio for myelinated fibers in the rat CNS? A theoretical approach. *PLoS ONE* **4**: e7754.
30. Baek, RC, Martin, DR, Cox, NR and Seyfried, TN (2009). Comparative analysis of brain lipids in mice, cats, and humans with Sandhoff disease. *Lipids* **44**: 197–205.
31. Agrawal, D, Hawk, R, Avila, RL, Inouye, H and Kirschner, DA (2009). Internodal myelination during development quantitated using X-ray diffraction. *J Struct Biol* **168**: 521–526.
32. Avila, RL, Inouye, H, Baek, RC, Yin, X, Trapp, BD, Feltri, ML *et al.* (2005). Structure and stability of internodal myelin in mouse models of hereditary neuropathy. *J Neuropathol Exp Neurol* **64**: 976–990.
33. Foust, KD, Wang, X, McGovern, VL, Braun, L, Bevan, AK, Haidet, AM *et al.* (2010). Rescue of the spinal muscular atrophy phenotype in a mouse model by early postnatal delivery of SMN. *Nat Biotechnol* **28**: 271–274.
34. Madhavarao, CN, Chinopoulos, C, Chandrasekaran, K and Namboodiri, MA (2003). Characterization of the N-acetylaspartate biosynthetic enzyme from rat brain. *J Neurochem* **86**: 824–835.
35. Madhavarao, CN, Moffett, JR, Moore, RA, Viola, RE, Namboodiri, MA and Jacobowitz, DM (2004). Immunohistochemical localization of aspartoacylase in the rat central nervous system. *J Comp Neurol* **472**: 318–329.
36. Kirmani, BF, Jacobowitz, DM, Kallarakal, AT and Namboodiri, MA (2002). Aspartoacylase is restricted primarily to myelin synthesizing cells in the CNS: therapeutic implications for Canavan disease. *Brain Res Mol Brain Res* **107**: 176–182.
37. Baslow, MH (2000). Functions of N-acetyl-L-aspartate and N-acetyl-L-aspartylglutamate in the vertebrate brain: role in glial cell-specific signaling. *J Neurochem* **75**: 453–459.
38. Mehta, V and Namboodiri, MA (1995). N-acetylaspartate as an acetyl source in the nervous system. *Brain Res Mol Brain Res* **31**: 151–157.
39. Kaul, R, Casanova, J, Johnson, AB, Tang, P and Matalon, R (1991). Purification, characterization, and localization of aspartoacylase from bovine brain. *J Neurochem* **56**: 129–135.
40. Goldstein, FB (1976). Amidohydrolases of brain; enzymatic hydrolysis of N-acetyl-L-aspartate and other N-acyl-L-amino acids. *J Neurochem* **26**: 45–49.
41. Gray, SJ, Nagabhushan Kalburgi, S, McCown, TJ and Jude Samulski, R (2013). Global CNS gene delivery and evasion of anti-AAV-neutralizing antibodies by intrathecal AAV administration in non-human primates. *Gene Ther* **20**: 450–459.
42. Wang, J, Leone, P, Wu, G, Francis, JS, Li, H, Jain, MR *et al.* (2009). Myelin lipid abnormalities in the aspartoacylase-deficient tremor rat. *Neurochem Res* **34**: 138–148.
43. Saher, G, Brügger, B, Lappe-Siefke, C, Möbius, W, Tozawa, R, Wehr, MC *et al.* (2005). High cholesterol level is essential for myelin membrane growth. *Nat Neurosci* **8**: 468–475.
44. Minutes of the Recombinant DNA Advisory Committee, 12/4/12–5/12 (2012). *Recombinant DNA Advisory Committee*. Bethesda, MD. pp. 9–10.
45. Sun, X, Lu, Y, Bish, LT, Calcedo, R, Wilson, JM and Gao, G (2010). Molecular analysis of vector genome structures after liver transduction by conventional and self-complementary adeno-associated viral serotype vectors in murine and nonhuman primate models. *Hum Gene Ther* **21**: 750–761.